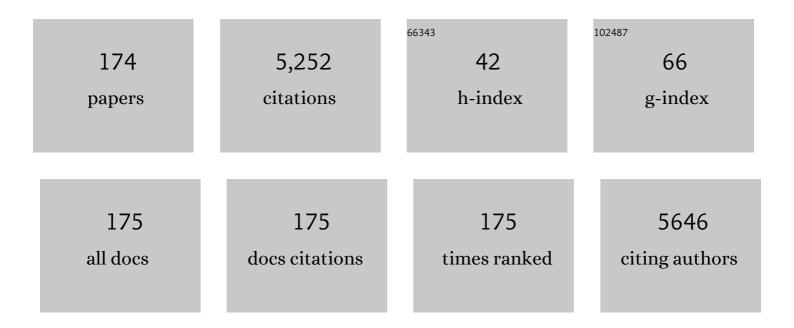
Chih-Kuang Yeh

List of Publications by Year in descending order

Source: https://exaly.com/author-pdf/3774799/publications.pdf Version: 2024-02-01



#	Article	IF	CITATIONS
1	Concurrent blood–brain barrier opening and local drug delivery using drug-carrying microbubbles and focused ultrasound for brain glioma treatment. Biomaterials, 2012, 33, 704-712.	11.4	239
2	Combining Microbubbles and Ultrasound for Drug Delivery to Brain Tumors: Current Progress and Overview. Theranostics, 2014, 4, 432-444.	10.0	229
3	Paclitaxel-liposome–microbubble complexes as ultrasound-triggered therapeutic drug delivery carriers. Journal of Controlled Release, 2013, 166, 246-255.	9.9	213
4	SPIO-conjugated, doxorubicin-loaded microbubbles for concurrent MRI and focused-ultrasound enhanced brain-tumor drug delivery. Biomaterials, 2013, 34, 3706-3715.	11.4	203
5	Aptamer-conjugated and drug-loaded acoustic droplets for ultrasound theranosis. Biomaterials, 2012, 33, 1939-1947.	11.4	177
6	Antiangiogenic-targeting drug-loaded microbubbles combined with focused ultrasound for glioma treatment. Biomaterials, 2013, 34, 2142-2155.	11.4	124
7	Non-invasive, neuron-specific gene therapy by focused ultrasound-induced blood-brain barrier opening in Parkinson's disease mouse model. Journal of Controlled Release, 2016, 235, 72-81.	9.9	119
8	Ultrasound/Magnetic Targeting with SPIO-DOX-Microbubble Complex for Image-Guided Drug Delivery in Brain Tumors. Theranostics, 2016, 6, 1542-1556.	10.0	108
9	Improving Nanoparticle Penetration in Tumors by Vascular Disruption with Acoustic Droplet Vaporization. Theranostics, 2016, 6, 392-403.	10.0	99
10	Characterization of Different Microbubbles in Assisting Focused Ultrasound-Induced Blood-Brain Barrier Opening. Scientific Reports, 2017, 7, 46689.	3.3	96
11	Focused Ultrasound-Induced Blood-Brain Barrier Opening: Association with Mechanical Index and Cavitation Index Analyzed by Dynamic Contrast-Enhanced Magnetic-Resonance Imaging. Scientific Reports, 2016, 6, 33264.	3.3	93
12	Tumortropic monocyte-mediated delivery of echogenic polymer bubbles and therapeutic vesicles for chemotherapy of tumor hypoxia. Biomaterials, 2015, 71, 71-83.	11.4	92
13	Noninvasive, Targeted and Non-Viral Ultrasound-Mediated GDNF-Plasmid Delivery for Treatment of Parkinson's Disease. Scientific Reports, 2016, 6, 19579.	3.3	91
14	Folate-conjugated gene-carrying microbubbles with focused ultrasound for concurrent blood-brain barrier opening and local gene delivery. Biomaterials, 2016, 106, 46-57.	11.4	88
15	Enhanced delivery of paclitaxel liposomes using focused ultrasound with microbubbles for treating nude mice bearing intracranial glioblastoma xenografts. International Journal of Nanomedicine, 2017, Volume 12, 5613-5629.	6.7	81
16	Focused ultrasound-induced blood-brain barrier opening for non-viral, non-invasive, and targeted gene delivery. Journal of Controlled Release, 2015, 212, 1-9.	9.9	79
17	Aptamer-Conjugated Nanobubbles for Targeted Ultrasound Molecular Imaging. Langmuir, 2011, 27, 6971-6976.	3.5	76
18	Potential-well model in acoustic tweezers. IEEE Transactions on Ultrasonics, Ferroelectrics, and Frequency Control, 2010, 57, 1451-1459.	3.0	70

#	Article	IF	CITATIONS
19	Synthesis and biological characterization of novel rose bengal derivatives with improved amphiphilicity for sono-photodynamic therapy. European Journal of Medicinal Chemistry, 2018, 145, 86-95.	5.5	69
20	Ultrasonic Nakagami Imaging: A Strategy to Visualize the Scatterer Properties of Benign and Malignant Breast Tumors. Ultrasound in Medicine and Biology, 2010, 36, 209-217.	1.5	68
21	Ultrasound targeted CNS gene delivery for Parkinson's disease treatment. Journal of Controlled Release, 2017, 261, 246-262.	9.9	68
22	Drug-loaded bubbles with matched focused ultrasound excitation for concurrent blood–brain barrier opening and brain-tumor drug delivery. Acta Biomaterialia, 2015, 15, 89-101.	8.3	67
23	Classification of Benign and Malignant Breast Tumors by 2-D Analysis Based on Contour Description and Scatterer Characterization. IEEE Transactions on Medical Imaging, 2010, 29, 513-522.	8.9	66
24	Classification of breast masses by ultrasonic Nakagami imaging: a feasibility study. Physics in Medicine and Biology, 2008, 53, 6027-6044.	3.0	64
25	Classification of scattering media within benign and malignant breast tumors based on ultrasound textureâ€featureâ€based and Nakagamiâ€parameter images. Medical Physics, 2011, 38, 2198-2207.	3.0	64
26	Angiogenesis-targeting microbubbles combined with ultrasound-mediated gene therapy in brain tumors. Journal of Controlled Release, 2017, 255, 164-175.	9.9	64
27	Superhydrophobic drug-loaded mesoporous silica nanoparticles capped with β-cyclodextrin for ultrasound image-guided combined antivascular and chemo-sonodynamic therapy. Biomaterials, 2020, 232, 119723.	11.4	64
28	Submicron-Bubble-Enhanced Focused Ultrasound for Blood–Brain Barrier Disruption and Improved CNS Drug Delivery. PLoS ONE, 2014, 9, e96327.	2.5	63
29	Intracellular Acoustic Droplet Vaporization in a Single Peritoneal Macrophage for Drug Delivery Applications. Langmuir, 2011, 27, 13183-13188.	3.5	59
30	A tumor-targeted activatable phthalocyanine-tetrapeptide-doxorubicin conjugate for synergistic chemo-photodynamic therapy. European Journal of Medicinal Chemistry, 2017, 127, 200-209.	5.5	59
31	Redox nanoparticle treatment protects against neurological deficit in focused ultrasound-induced intracerebral hemorrhage. Nanomedicine, 2012, 7, 1029-1043.	3.3	58
32	Ultrasound with microbubbles improves memory, ameliorates pathology and modulates hippocampal proteomic changes in a triple transgenic mouse model of Alzheimer's disease. Theranostics, 2020, 10, 11794-11819.	10.0	55
33	Ultrasound in tumor immunotherapy: Current status and future developments. Journal of Controlled Release, 2020, 323, 12-23.	9.9	55
34	Superhydrophobic silica nanoparticles as ultrasound contrast agents. Ultrasonics Sonochemistry, 2017, 36, 262-269.	8.2	53
35	Sonogenetic Modulation of Cellular Activities Using an Engineered Auditory-Sensing Protein. Nano Letters, 2020, 20, 1089-1100.	9.1	52
36	Detection of Intracerebral Hemorrhage and Transient Blood-Supply Shortage in Focused-Ultrasound-Induced Blood–Brain Barrier Disruption by Ultrasound Imaging. Ultrasound in Medicine and Biology, 2012, 38, 1372-1382.	1.5	51

#	Article	IF	CITATIONS
37	Tornado-inspired acoustic vortex tweezer for trapping and manipulating microbubbles. Proceedings of the National Academy of Sciences of the United States of America, 2021, 118, .	7.1	51
38	Targeted tumor theranostics using folate-conjugated and camptothecin-loaded acoustic nanodroplets in a mouse xenograft model. Biomaterials, 2015, 53, 699-708.	11.4	50
39	Hepatic Steatosis Assessment with Ultrasound Small-Window Entropy Imaging. Ultrasound in Medicine and Biology, 2018, 44, 1327-1340.	1.5	50
40	Assessment of Median Nerve Mobility by Ultrasound Dynamic Imaging for Diagnosing Carpal Tunnel Syndrome. PLoS ONE, 2016, 11, e0147051.	2.5	49
41	Mechanical bioeffects of acoustic droplet vaporization in vessel-mimicking phantoms. Ultrasonics Sonochemistry, 2014, 21, 1866-1874.	8.2	47
42	Concurrent anti-vascular therapy and chemotherapy in solid tumors using drug-loaded acoustic nanodroplet vaporization. Acta Biomaterialia, 2017, 49, 472-485.	8.3	46
43	Normalization of Tumor Vasculature by Oxygen Microbubbles with Ultrasound. Theranostics, 2019, 9, 7370-7383.	10.0	44
44	Contrast-Enhanced Ultrasound Imaging for the Detection of Focused Ultrasound-Induced Blood-Brain Barrier Opening. Theranostics, 2014, 4, 1014-1025.	10.0	43
45	Ultrasound microbubble contrast agents for diagnostic and therapeutic applications : current status and future design. Biomedical Journal, 2012, 35, 125.	3.1	43
46	Effects of Acoustic Insonation Parameters on Ultrasound Contrast Agent Destruction. Ultrasound in Medicine and Biology, 2008, 34, 1281-1291.	1.5	42
47	Superparamagnetic iron oxide and drug complex-embedded acoustic droplets for ultrasound targeted theranosis. Biomaterials, 2013, 34, 1852-1861.	11.4	42
48	Theranostic Performance of Acoustic Nanodroplet Vaporization-Generated Bubbles in Tumor Intertissue. Theranostics, 2017, 7, 1477-1488.	10.0	42
49	Focused ultrasound-induced blood brain-barrier opening enhanced vascular permeability for GDNF delivery in Huntington's disease mouse model. Brain Stimulation, 2019, 12, 1143-1150.	1.6	40
50	Inertial cavitation initiated by polytetrafluoroethylene nanoparticles under pulsed ultrasound stimulation. Ultrasonics Sonochemistry, 2016, 32, 1-7.	8.2	39
51	Enhancing Boron Uptake in Brain Glioma by a Boron-Polymer/Microbubble Complex with Focused Ultrasound. ACS Applied Materials & Interfaces, 2019, 11, 11144-11156.	8.0	39
52	A Simple Method for Quantifying Ultrasound-Triggered Microbubble Destruction. Ultrasound in Medicine and Biology, 2011, 37, 949-957.	1.5	38
53	Characterization of Acoustic Droplet Vaporization for Control of Bubble Generation Under Flow Conditions. Ultrasound in Medicine and Biology, 2014, 40, 551-561.	1.5	38
54	Spatially Uniform Tumor Treatment and Drug Penetration by Regulating Ultrasound with Microbubbles. ACS Applied Materials & Interfaces, 2018, 10, 17784-17791.	8.0	38

#	Article	IF	CITATIONS
55	Carpal Tunnel Syndrome: US Strain Imaging for Diagnosis. Radiology, 2015, 275, 205-214.	7.3	36
56	Near Infraredâ€Activatable Platinumâ€Decorated Gold Nanostars for Synergistic Photothermal/Ferroptotic Therapy in Combating Cancer Drug Resistance. Advanced Healthcare Materials, 2020, 9, e2000864.	7.6	36
57	Current progress in antivascular tumor therapy. Drug Discovery Today, 2017, 22, 1503-1515.	6.4	35
58	Theranostic nanosensitizers for highly efficient <scp>MR</scp> /fluorescence imagingâ€guided sonodynamic therapy of gliomas. Journal of Cellular and Molecular Medicine, 2018, 22, 5394-5405.	3.6	34
59	Biomimetic Acoustically-Responsive Vesicles for Theranostic Applications. Theranostics, 2015, 5, 1264-1274.	10.0	32
60	Development of a Novel Hanging Drop Platform for Engineering Controllable 3D Microenvironments. Frontiers in Cell and Developmental Biology, 2020, 8, 327.	3.7	31
61	Multifeature analysis of an ultrasound quantitative diagnostic index for classifying nonalcoholic fatty liver disease. Scientific Reports, 2016, 6, 35083.	3.3	30
62	C-Phycocyanin as a tumour-associated macrophage-targeted photosensitiser and a vehicle of phthalocyanine for enhanced photodynamic therapy. Chemical Communications, 2017, 53, 4112-4115.	4.1	30
63	In vivo imaging of blood flow in the mouse Achilles tendon using high-frequency ultrasound. Ultrasonics, 2009, 49, 226-230.	3.9	27
64	High-Resolution Functional Vascular Assessment With Ultrasound. IEEE Transactions on Medical Imaging, 2004, 23, 1263-1275.	8.9	25
65	Strainâ€compounding technique with ultrasound Nakagami imaging for distinguishing between benign and malignant breast tumors. Medical Physics, 2012, 39, 2325-2333.	3.0	25
66	On velocity estimation using speckle decorrelation [blood]. IEEE Transactions on Ultrasonics, Ferroelectrics, and Frequency Control, 2001, 48, 1084-1091.	3.0	24
67	Rapid Transformation of Protein-Caged Nanomaterials into Microbubbles As Bimodal Imaging Agents. ACS Nano, 2012, 6, 5111-5121.	14.6	23
68	Camptothecin-loaded fusogenic nanodroplets as ultrasound theranostic agent in stem cell-mediated drug-delivery system. Journal of Controlled Release, 2018, 278, 100-109.	9.9	23
69	Ultrasound Entropy Imaging of Nonalcoholic Fatty Liver Disease: Association with Metabolic Syndrome. Entropy, 2018, 20, 893.	2.2	23
70	Microbubble-enhanced Focused Ultrasound-induced Blood–brain Barrier Opening for Local and Transient Drug Delivery in Central Nervous System Disease. Journal of Medical Ultrasound, 2014, 22, 183-193.	0.4	22
71	Microcirculation volumetric flow assessment using high-resolution, contrast-assisted images. IEEE Transactions on Ultrasonics, Ferroelectrics, and Frequency Control, 2008, 55, 74-83.	3.0	21
72	Macrophages as Drug Delivery Carriers for Acoustic Phase-Change Droplets. Ultrasound in Medicine and Biology, 2018, 44, 1468-1481.	1.5	21

#	Article	IF	CITATIONS
73	Spatial-Temporal Cellular Bioeffects from Acoustic Droplet Vaporization. Theranostics, 2018, 8, 5731-5743.	10.0	21
74	Targeted delivery of engineered auditory sensing protein for ultrasound neuromodulation in the brain. Theranostics, 2020, 10, 3546-3561.	10.0	21
75	Gelatin scaffold with multifunctional curcumin-loaded lipid-PLGA hybrid microparticles for regenerating corneal endothelium. Materials Science and Engineering C, 2021, 120, 111753.	7.3	20
76	Microbubbles: A Novel Strategy for Chemotherapy. Current Pharmaceutical Design, 2017, 23, 3383-3390.	1.9	20
77	Thermal-sensitive acoustic droplets for dual-mode ultrasound imaging and drug delivery. Journal of Controlled Release, 2018, 291, 26-36.	9.9	19
78	Sonogenetic-Based Neuromodulation for the Amelioration of Parkinson's Disease. Nano Letters, 2021, 21, 5967-5976.	9.1	19
79	Assessment of tumor vasculature for diagnostic and therapeutic applications in a mouse model in vivo using 25-MHz power Doppler imaging. Ultrasonics, 2011, 51, 925-931.	3.9	18
80	A maleimide-based in-vitro model for ultrasound targeted imaging. Ultrasonics Sonochemistry, 2011, 18, 327-333.	8.2	18
81	Ultrasound-Induced Magnetic Imaging of Tumors Targeted by Biofunctional Magnetic Nanoparticles. ACS Nano, 2017, 11, 3030-3037.	14.6	18
82	Ultrasound imaging in nonalcoholic liver disease: current applications and future developments. Quantitative Imaging in Medicine and Surgery, 2019, 9, 546-551.	2.0	18
83	A preliminary study of Parkinson's gene therapy via sono-magnetic sensing gene vector for conquering extra/intracellular barriers in mice. Brain Stimulation, 2020, 13, 786-799.	1.6	18
84	Ultrasound-activated nanomaterials for sonodynamic cancer theranostics. Drug Discovery Today, 2022, 27, 1590-1603.	6.4	18
85	Dual high-frequency difference excitation for contrast detection. IEEE Transactions on Ultrasonics, Ferroelectrics, and Frequency Control, 2008, 55, 2164-2176.	3.0	17
86	Concurrent Osteosarcoma Theranostic Strategy Using Contrast-Enhanced Ultrasound and Drug-Loaded Bubbles. Pharmaceutics, 2019, 11, 223.	4.5	16
87	Contrast-specific ultrasonic flow measurements based on both input and output time intensities. Ultrasound in Medicine and Biology, 2003, 29, 671-678.	1.5	15
88	Drug-carrying microbubbles as a theranostic tool in convection-enhanced delivery for brain tumor therapy. Oncotarget, 2017, 8, 42359-42371.	1.8	15
89	Texture Feature Analysis for Breast Ultrasound Image Enhancement. Ultrasonic Imaging, 2011, 33, 264-278.	2.6	14
90	Ultrasonic technologies in imaging and drug delivery. Cellular and Molecular Life Sciences, 2021, 78, 6119-6141.	5.4	14

#	Article	IF	CITATIONS
91	Doppler angle estimation using AR modeling. IEEE Transactions on Ultrasonics, Ferroelectrics, and Frequency Control, 2002, 49, 683-692.	3.0	13
92	Ultrasound-Enhanced Protective Effect of Tetramethylpyrazine via the ROS/HIF-1A Signaling Pathway in an in Vitro Cerebral Ischemia/Reperfusion Injury Model. Ultrasound in Medicine and Biology, 2018, 44, 1786-1798.	1.5	13
93	Internal polymer scaffolding in lipid-coated microbubbles for control of inertial cavitation in ultrasound theranostics. Journal of Materials Chemistry B, 2015, 3, 5938-5941.	5.8	12
94	Roles of Textural and Surface Properties of Nanoparticles in Ultrasound-Responsive Systems. Langmuir, 2018, 34, 1256-1265.	3.5	12
95	Oscillatory behavior of microbubbles impacts efficacy of cellular drug delivery. Journal of Controlled Release, 2021, 333, 316-327.	9.9	12
96	Feasibility Exploration of Blood Flow Estimation by Contrast-Assisted Nakagami Imaging. Ultrasonic Imaging, 2008, 30, 133-150.	2.6	11
97	Microbubble destruction by dual-high-frequency ultrasound excitation. IEEE Transactions on Ultrasonics, Ferroelectrics, and Frequency Control, 2009, 56, 1113-1118.	3.0	11
98	A Preclinical Study to Explore Vasculature Differences Between Primary and Recurrent Tumors Using Ultrasound Doppler Imaging. Ultrasound in Medicine and Biology, 2013, 39, 860-869.	1.5	11
99	Improvement of light penetration in biological tissue using an ultrasound-induced heating tunnel. Scientific Reports, 2020, 10, 17406.	3.3	11
100	Controlling the Size Distribution of Lipid-Coated Bubbles via Fluidity Regulation. Ultrasound in Medicine and Biology, 2013, 39, 882-892.	1.5	10
101	Trapping of a mie sphere by acoustic pulses: effects of pulse length. IEEE Transactions on Ultrasonics, Ferroelectrics, and Frequency Control, 2013, 60, 1487-1497.	3.0	9
102	Dual-frequency chirp imaging for contrast detection. Physics in Medicine and Biology, 2011, 56, 2767-2778.	3.0	8
103	Characterization of tumor vasculature distributions in central and peripheral regions based on Doppler ultrasound. Medical Physics, 2012, 39, 7490-7498.	3.0	8
104	Skin-scanning technique for superficial blood flow imaging using a high-frequency ultrasound system. Ultrasonics, 2014, 54, 241-246.	3.9	8
105	Manipulating Cellular Activities Using an Ultrasound–Chemical Hybrid Tool. ACS Synthetic Biology, 2017, 6, 2021-2027.	3.8	8
106	Characterization of limb lymphedema using the statistical analysis of ultrasound backscattering. Quantitative Imaging in Medicine and Surgery, 2020, 10, 48-56.	2.0	8
107	Dual-high-frequency ultrasound excitation on microbubble destruction volume. Ultrasonics, 2010, 50, 698-703.	3.9	7
108	Efficacy of Quantitative Muscle Ultrasound Using Texture-Feature Parametric Imaging in Detecting Pompe Disease in Children. Entropy, 2019, 21, 714.	2.2	7

Chih-Kuang Yeh

#	Article	IF	CITATIONS
109	Doppler Angle Estimation of Pulsatile Flows Using AR Modeling. Ultrasonic Imaging, 2002, 24, 65-80.	2.6	6
110	Amplitude-Modulation Chirp Imaging for Contrast Detection. Ultrasound in Medicine and Biology, 2010, 36, 1535-1545.	1.5	6
111	Discrimination of breast microcalcifications using a strain-compounding technique with ultrasound speckle factor imaging. IEEE Transactions on Ultrasonics, Ferroelectrics, and Frequency Control, 2014, 61, 955-965.	3.0	6
112	Assessment of temporary cerebral effects induced by focused ultrasound with optical coherence tomography angiography. Biomedical Optics Express, 2018, 9, 507.	2.9	6
113	Metabolic Characteristics of a Novel Ultrasound Quantitative Diagnostic Index for Nonalcoholic Fatty Liver Disease. Scientific Reports, 2019, 9, 7922.	3.3	6
114	Dynamic Ultrasound Assessment of Median Nerve Mobility Changes Following Corticosteroid Injection and Carpal Tunnel Release in Patients With Carpal Tunnel Syndrome. Frontiers in Neurology, 2021, 12, 710511.	2.4	6
115	Dynamic perfusion assessment by contrast-enhanced ultrasound in blood-brain barrier disruption. , 2013, 2013, 1152-5.		5
116	3-D Ultrafast Ultrasound Imaging of Microbubbles Trapped Using an Acoustic Vortex. IEEE Transactions on Ultrasonics, Ferroelectrics, and Frequency Control, 2021, 68, 3507-3514.	3.0	5
117	Carpal tunnel syndrome diagnosis by a selfâ€normalization process and ultrasound compound imaging. Medical Physics, 2012, 39, 7402-7411.	3.0	4
118	Realâ€ŧime monitoring of inertial cavitation effects of microbubbles by using MRI: In vitro experiments. Magnetic Resonance in Medicine, 2017, 77, 102-111.	3.0	4
119	Dual-Frequency Chirp Excitation for Passive Cavitation Imaging in the Brain. IEEE Transactions on Ultrasonics, Ferroelectrics, and Frequency Control, 2020, 67, 1127-1140.	3.0	4
120	Focused Ultrasound with Submicron Bubbles Producing Inertial Cavitation Suppression in Blood-Brain Barrier Opening Application. , 2011, , .		3
121	Ultrasonic Transdermal Delivery System with Acid–Base Neutralization-Generated CO ₂ Microbubble Cavitation. ACS Applied Bio Materials, 2020, 3, 1968-1975.	4.6	3
122	The Impact of Surface Drug Distribution on the Acoustic Behavior of DOX-Loaded Microbubbles. Pharmaceutics, 2021, 13, 2080.	4.5	3
123	Overcoming Hypoxia-Induced Drug Resistance via Promotion of Drug Uptake and Reoxygenation by Acousto–Mechanical Oxygen Delivery. Pharmaceutics, 2022, 14, 902.	4.5	3
124	A theoretical time-course model of acoustic tweezers: Pulse-wave mode. , 2008, , .		2
125	Classification of benign and malignant breast tumors by the contour analysis and scatterers characterization. , 2009, , .		2
126	DNA-conjugated gold nanoparticles for ultrasound targeted drug delivery. , 2012, , .		2

#	Article	IF	CITATIONS
127	Fabrication of through-silicon vias (TSV) by nickel electroplating in supercritical CO <inf>2</inf> . , 2014, , .		2
128	Transverse manipulation of microbubbles using acoustic-vortex tweezers. , 2015, , .		2
129	Template-based formation of ultrasound microbubble contrast agents. RSC Advances, 2016, 6, 69185-69190.	3.6	2
130	Monitoring of acoustic cavitation in microbubbleâ€presented focused ultrasound exposure using gradientâ€echo MRI. Journal of Magnetic Resonance Imaging, 2020, 51, 311-318.	3.4	2
131	Exploring the Acoustic and Dynamic Characteristics of Phase-Change Droplets. IEEE Transactions on Ultrasonics, Ferroelectrics, and Frequency Control, 2021, 68, 1051-1061.	3.0	2
132	Contrast-based ultrasonic blood flow measurements based on inflow/outflow time intensities. , 0, , .		1
133	Characterization of tumor vasculature derived from angiogenesis and vasculogenesis by high-frequency three-dimensional Doppler ultrasound. , 2010, , .		1
134	Dual-frequency excitation enhances targeted delivery of ultrasound microbubbles. , 2010, , .		1
135	An integrated approach based on morphology, texture, and backscattering-statistics for distinguishing between benign and malignant breast. , 2010, , .		1
136	Delivery of drug-loaded microbubbles and disruption of blood-brain barrier by focused ultrasound in a xenograft rat glioma model. , 2011, , .		1
137	Using fluidity regulation to control size distribution of lipid-coated bubbles. , 2011, , .		1
138	Superparamagnetic iron oxide/drug complex-embedded droplets for Bi-model imaging and enhanced targeted therapy. , 2012, , .		1
139	Phantom investigation of phase-inversion-based dual-frequency excitation imaging for improved contrast display. Ultrasonics, 2012, 52, 25-32.	3.9	1
140	Assessment of median nerve mobility by ultrasound dynamic imaging in carpal tunnel syndrome diagnosis. , 2013, , .		1
141	Using microbubbles as an MRI contrast agent for the measurement of cerebral blood volume. NMR in Biomedicine, 2013, 26, 1540-1546.	2.8	1
142	High-speed fluorescence imaging of ultrasound-triggered drug release from phase-change droplets. , 2014, , .		1
143	Sonogenetic Modulation of Cellular Activities in Mammalian Cells. Methods in Molecular Biology, 2021, 2312, 109-124.	0.9	1

144 Doppler angle estimation using the AR spectrum model. , 0, , .

0

#	Article	IF	CITATIONS
145	A compound ultrasound imaging strategy in carpel tunnel syndrome diagnosis. , 2008, , .		0
146	Microbubble detection by dual-high-frequency ultrasound excitation. , 2008, , .		0
147	Detection of blood-brain barrier disruption by contrast-enhanced high frequency ultrasound image: Small animals study. , 2009, , .		0
148	Phase-dependent dual-frequency contrast imaging. , 2009, , .		0
149	Detection of transient ischemia and hemorrhage in blood-brain barrier disruption by high-frequency ultrasound imaging. , 2010, , .		0
150	One-step covalently conjugated aptamer microbubbles for ultrasound targeted imaging. , 2010, , .		0
151	Feasibility study of using macrophages as drug delivery carriers for drug-loaded phase-change droplets. , 2011, , .		0
152	Acoustically-triggered droplet vaporization in macrophages for hypoxic-tumor therapy. , 2011, , .		0
153	A targeting therapy strategy by aptamer-conjugated and drug-loaded droplets. , 2011, , .		0
154	Characterize the vasculatures distribution of murine tumors between center and peripheral regions based on doppler ultrasound and immunofluorescent analysis. , 2011, , .		0
155	Effects of acoustic parameters on acoustically-vaporized droplets under dynamics flow conditions. , 2012, , .		0
156	Superparamagnetic iron-oxide drug-loading microbubbles for concurrent magnetic resonance imaging monitoring and focused-ultrasound enhanced brain-tumor drug delivery. , 2012, , .		0
157	Erosion of tissue-mimicking phantom by acoustic droplet vaporization. , 2012, , .		0
158	Targeted drug-loading microbubbles with focused ultrasound induced blood-brain barrier disruption for glioma treatment. , 2012, , .		0
159	Contrast-enhanced ultrasound imaging for the detection of transient dynamics of blood-brain barrier opening induced by focused ultrasound. , 2013, , .		0
160	High-sensitivity distribution mapping of iron, zinc and copper during spio-microbubbles facilitated focused ultrasound induced blood-brain barrier opening via laser ablation/inductively coupled plasma mass spectrometry. , 2013, , .		0
161	Effects of ultrasound parameters on the acoustic characteristics of phase-change droplets. , 2014, , .		0
162	Regulating nonlinear properties of lipid-coated microbubbles using polymer network scaffolds for ultrasound drug delivery applications. , 2014, , .		0

#	Article	IF	CITATIONS
163	Ultrasound-mediated gene delivery by using folic acid-modified cationic microbubbles. , 2014, , .		Ο
164	High-speed fluorescence microscopy of near-wall shedding of drug-lipid complexes from phase-change droplets. , 2015, , .		0
165	Ultrasound-triggered and targeted gene delivery by using cationic microbubbles to enhance GDNF gene transfection in a rat Parkinson's disease model. , 2015, , .		Ο
166	Improvement of drug penetration in solid tumors by vascular disruption with acoustic nanodroplet vaporization. , 2015, , .		0
167	SPIO-DOX-microbubble complex with ultrasound for MRI image-guided drug delivery in a rat glioma model. , 2016, , .		Ο
168	Superhydrophobic mesoporous silica nanoparticles as ultrasound contrast agents. , 2016, , .		0
169	Notice of Removal: Ultrasound-chemical hybrid system for manipulating cellular activities. , 2017, , .		Ο
170	Notice of Removal: A preliminary study of Amorphous calcium carbonate-Doxorubicin nanoparticles (ACC-DOX NPs) for ultrasound theraonstics. , 2017, , .		0
171	Notice of Removal: Concurrent anti-vascular, sonodynamic and chemo therapy in solid tumors by superhydrophobic dox-loaded nanoparticles. , 2017, , .		Ο
172	Notice of Removal: Feasibility study of dual-frequency chirp excitation for passive cavitation imaging. , 2017, , .		0
173	Notice of Removal: Bioeffects of acoustic droplet vaporization-generated bubbles in tissue. , 2017, , .		Ο
174	Ultrasound-guided system for light focusing using microbubbles generated from polytetrafluoroethylene nanoparticles. Applied Physics Letters, 2022, 120, 053701.	3.3	0